



Correction to "Extensive MRO CRISM observations of 1.27 μm O₂ airglow in Mars polar night and their comparison to MRO MCS temperature profiles and LMD GCM simulations"

R. Todd Clancy, Brad J. Sandor, Michael J. Wolff, Michael D. Smith, Franck Lefèvre, Jean-Baptiste Madeleine, François Forget, Scott L. Murchie, Frank Seelos, Kim D. Seelos, et al.

► To cite this version:

R. Todd Clancy, Brad J. Sandor, Michael J. Wolff, Michael D. Smith, Franck Lefèvre, et al.. Correction to "Extensive MRO CRISM observations of 1.27 μm O₂ airglow in Mars polar night and their comparison to MRO MCS temperature profiles and LMD GCM simulations". Journal of Geophysical Research. Planets, 2013, 118 (5), pp.1148-1154. 10.1002/jgre.20073 . hal-00835880

HAL Id: hal-00835880

<https://hal.science/hal-00835880>

Submitted on 29 Mar 2021

HAL is a multi-disciplinary open access archive for the deposit and dissemination of scientific research documents, whether they are published or not. The documents may come from teaching and research institutions in France or abroad, or from public or private research centers.

L'archive ouverte pluridisciplinaire **HAL**, est destinée au dépôt et à la diffusion de documents scientifiques de niveau recherche, publiés ou non, émanant des établissements d'enseignement et de recherche français ou étrangers, des laboratoires publics ou privés.

Correction to “Extensive MRO CRISM observations of 1.27 μm O₂ airglow in Mars polar night and their comparison to MRO MCS temperature profiles and LMD GCM simulations”

R. Todd Clancy,¹ Brad J. Sandor,¹ Michael J. Wolff,¹ Michael D. Smith,² Franck Lefèvre,³ Jean-Baptiste Madeleine,⁴ Francois Forget,⁴ Scott L. Murchie,⁵ Frank P. Seelos,⁵ Kim D. Seelos,⁵ Hari Nair,⁵ Anthony D. Toigo,⁵ David Humm,⁵ David M. Kass,⁶ Armin Kleinböhl,⁶ and Nicholas Heavens⁷

Received 13 February 2013; accepted 11 March 2013; published 3 May 2013.

Citation: Clancy, R. T., et al. (2013), Correction to “Extensive MRO CRISM observations of 1.27 μm O₂ airglow in Mars polar night and their comparison to MRO MCS temperature profiles and LMD GCM simulations,” *J. Geophys. Res. Planets*, 118, 1148–1154, doi:10.1002/jgre.20073.

1. Correction to Retrieved VER

[1] The scaling of CRISM (Compact Reconnaissance Imaging Spectrometer for Mars) retrieved O₂($^1\Delta_g$) 1.27 μm volume emission rate (VER) profiles, as plotted in Figures 7–17 and 21 of Clancy *et al.* [2012], includes a calibration error specific to the profile matrix inversion. Hence, all of the presented CRISM O₂($^1\Delta_g$) VER values should be decreased by a factor of 2.1. This error does not affect limb radiance values, such as presented in Figures 3–7, but significantly affects reported values for volume and vertically integrated emission rates. Vertically (46–75 km) integrated, latitudinally (70–90 NS) averaged O₂($^1\Delta_g$) emission rates of 250–300 kR are correctly calculated from CRISM winter polar nightglow observations. This error also impacts the conclusion that Laboratoire de Météorologie Dynamique general circulation/photochemical model [e.g., Lefèvre *et al.*, 2004] simulations of polar winter O₂($^1\Delta_g$) 1.27 μm VER are 40% lower, on average, than CRISM retrieved values. With the corrected profile scaling, Laboratoire de Météorologie Dynamique model O₂($^1\Delta_g$) VER are 25% higher than CRISM retrieved values, on average. Hence, the model-data disagreement is less than originally reported, and the model simulations appear to slightly overpredict, rather than under-predict, poleward upper level transport into the polar winter regions. All other conclusions associated with the presented O₂($^1\Delta_g$) model-data comparisons regard

variations (vertical, seasonal, latitudinal, local time, temperature dependence), and are generally unaffected by this correction. Corrected Figures 7–17 and 21 are provided below. The incorrect scaling of VER in Clancy *et al.* [2012] was strictly the fault of the lead author.

References

- Clancy, R.T., et al. (2012), Extensive MRO CRISM observations of 1.27 μm O₂ airglow in Mars polar night and their comparison to MRO MCS temperature profiles and LMD GCM simulations, *J. Geophys. Res.*, 117, E00J10, doi:10.1029/2011JE004018.
 Lefèvre, F., S. Lebonnois, F. Montmessin, and F. Forget (2004), Three-dimensional modeling of ozone on Mars, *J. Geophys. Res.*, 109, doi:10.1029/2004JE002268.

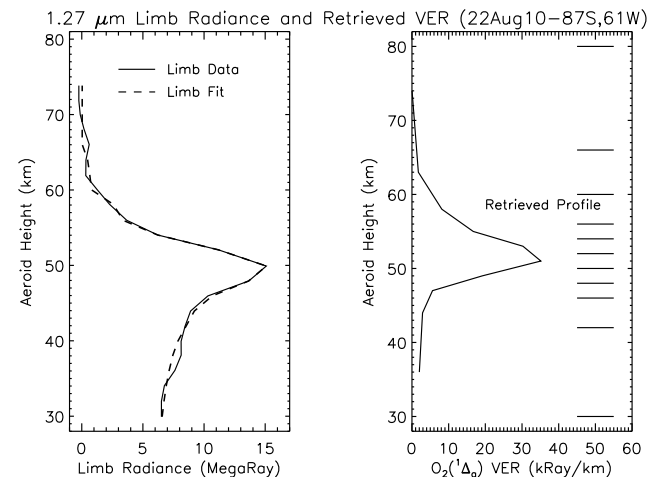


Figure 7. A nonlinear matrix inversion is adopted to invert CRISM limb radiance profiles of integrated O₂($^1\Delta_g$) 1.27 μm band emission (left panel) to vertical profiles of 1.27 μm volume emission rates (VER in kilo Rayleighs/km, right panel). The solid line in the left panel compares the observed 1.27 μm band emission for an August 2010 limb observation ($L_s = 137^\circ$) against the RT model limb radiance profile (dashed line) associated with the retrieved 1.27 μm VER (solid line in right panel). The solution retrieved VER profile is specified for discrete vertical layers indicated by horizontal lines at the right side of the right panel.

¹Space Science Institute, Boulder, Colorado, USA.

²Goddard Space Flight Center, Greenbelt, Maryland, USA.

³Laboratoire Atmosphères Milieux Observations Spatiales, Paris, France.

⁴Laboratoire de Météorologie Dynamique, Paris, France.

⁵Johns Hopkins University/Applied Physics Laboratory, Columbia, Maryland, USA.

⁶Jet Propulsion Laboratory, Pasadena, California, USA.

⁷Hampton University, Hampton, Virginia, USA.

Corresponding author: R. T. Clancy, Space Science Institute, Boulder, CO, USA. (clancy@spacescience.org)

©2013. American Geophysical Union. All Rights Reserved.
 2169-9097/13/10.1002/jgre.20073

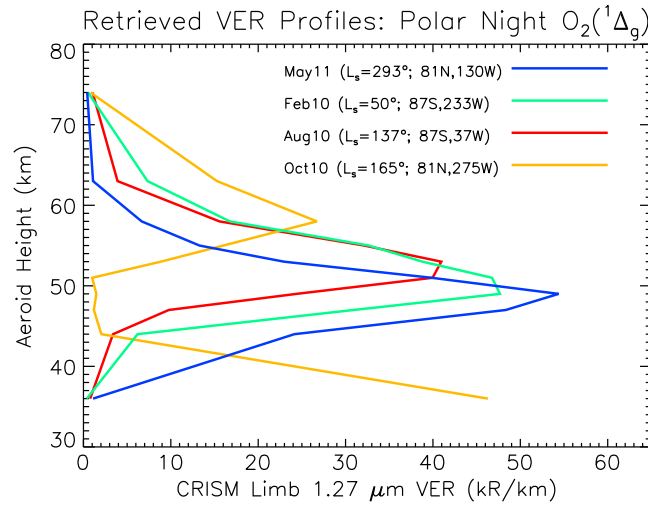


Figure 8. Vertical profiles of retrieved O₂(¹Δ_g) 1.27 μm VER are presented for the four CRISM limb radiance observations presented in Figure 5.

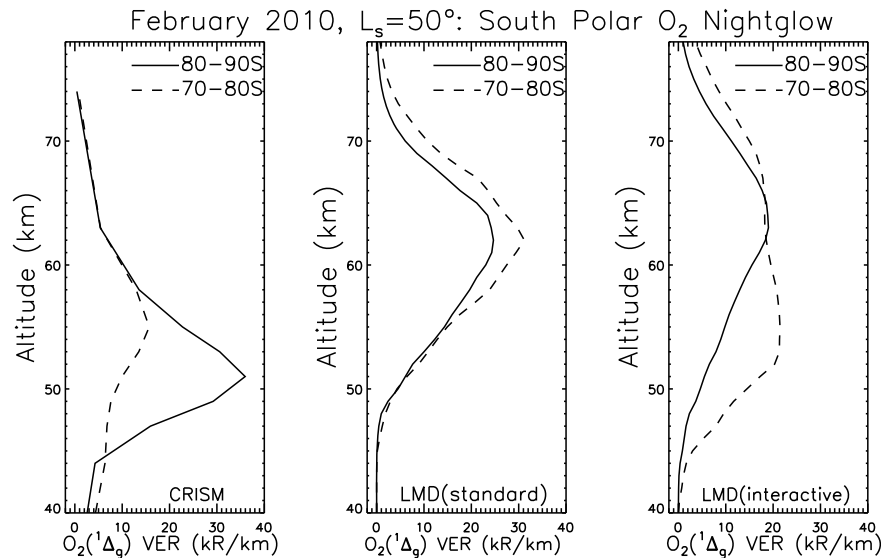


Figure 9. Averaged O₂(¹Δ_g) volume emission profiles (VER) from: (1) left panel, all CRISM retrievals on 10–11 February 2010 ($L_s = 50^\circ$) for latitude bins of 70°S–80°S (dashed lines) and 80°S–90°S (solid lines); (2) middle panel, standard LMD GCM simulations colocated and contemporaneous with each CRISM measurement for the same latitude bins; (3) right panel, interactive aerosol LMD GCM simulations colocated and contemporaneous with each CRISM measurement for the same latitude bins in this late southern fall season.

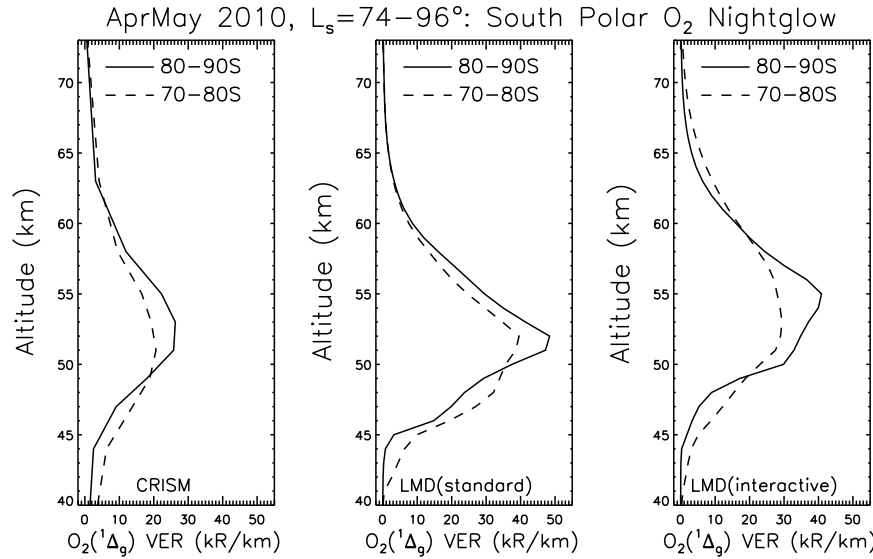


Figure 10. Averaged O₂(¹Δ_G) volume emission profiles (VER) from: (1) left panel, all CRISM retrievals on 7, 28–29 April and 26 May 2010 ($L_s = 74\text{--}96^\circ$) for latitude bins of 70°S–80°S (dashed lines) and 80°S–90°S (solid lines); (2) middle panel, standard LMD GCM simulations colocated and contemporaneous with each CRISM measurement for the same latitude bins; (3) right panel, interactive aerosol LMD GCM simulations co-located and contemporaneous with each CRISM measurement for the same latitude bins in this southern winter solstice season.

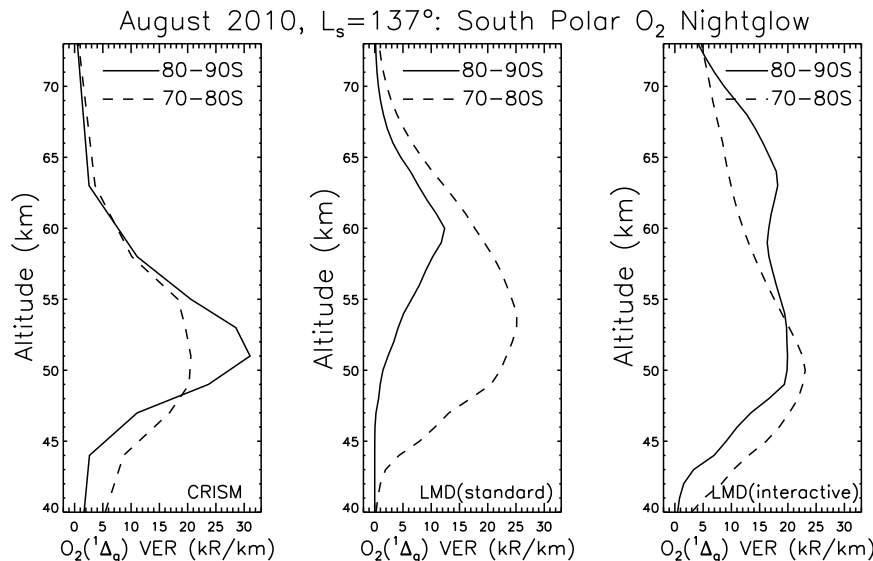


Figure 11. Averaged O₂(¹Δ_G) volume emission profiles (VER) from: (1) left panel, all CRISM retrievals on 22–23 August 2010 ($L_s = 137^\circ$) for latitude bins of 70°S–80°S (dashed lines) and 80°S–90°S (solid lines); (2) middle panel, standard LMD GCM simulations colocated and contemporaneous with each CRISM measurement for the same latitude bins; (3) right panel, interactive aerosol LMD GCM simulations colocated and contemporaneous with each CRISM measurement for the same latitude bins in this late southern winter season.

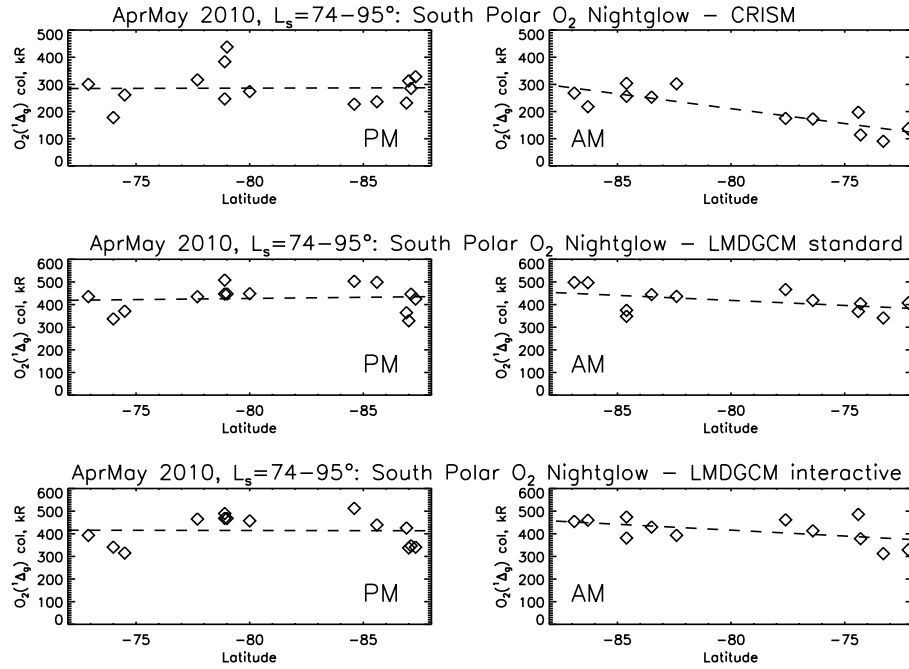


Figure 12. The latitudinal dependences of vertically integrated O₂(¹Δ_G) VER (~nadir VER, see text) are presented for P.M. (left panels) and A.M. (right panels) local times; for CRISM observations (top panels), and standard (middle panels) and interactive aerosol (bottom panels) model simulations for the April–May period of CRISM observations ($L_s = 74\text{--}95^\circ$). Dashed lines represent least-squares linear fits to the latitudinal/diurnal trends. Both observations and model O₂(¹Δ_G) VER are fairly constant across P.M. latitudes to the pole, but decrease from the pole to lower A.M. latitudes in a fairly monotonic fashion.

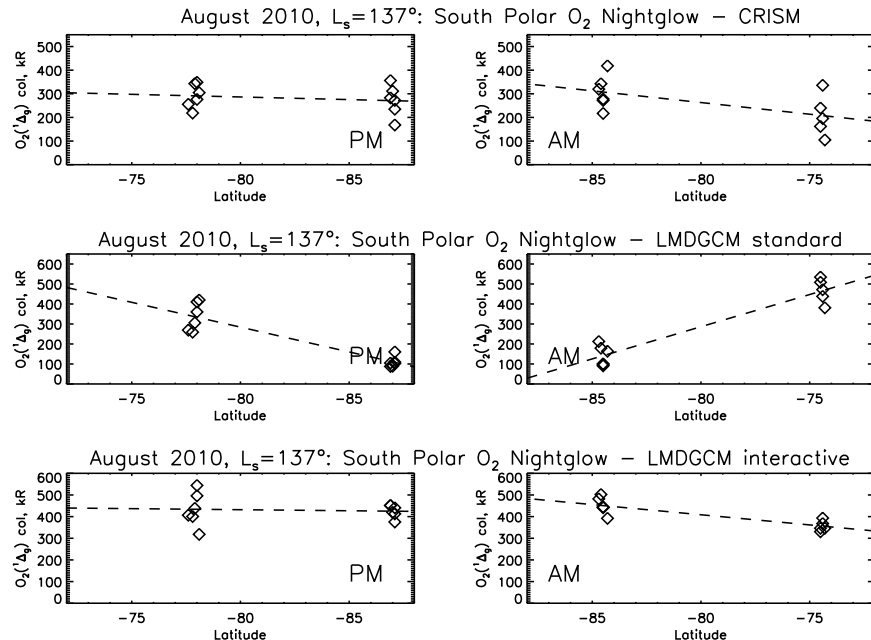


Figure 13. The latitudinal dependences of vertically integrated O₂(¹Δ_G) VER (~nadir VER, see text) are presented for P.M. (left panels) and A.M. (right panels) local times, for CRISM observations (top panels), and standard (middle panels) and interactive aerosol (bottom panels) model simulations for the August period of CRISM observations ($L_s = 137^\circ$). Dashed lines represent least-squares linear fits to the latitudinal/diurnal trends. Similar to the April–May ($L_s = 74\text{--}95^\circ$) behavior, the observations and interactive aerosol model O₂(¹Δ_G) VER are fairly constant across PM latitudes to the pole, but decrease from the pole to lower A.M. latitudes. In contrast, the standard model O₂(¹Δ_G) VER (middle panels) exhibit a distinctive, deep minimum in O₂(¹Δ_G) emission near the southern winter pole, coupled with diurnal symmetry.

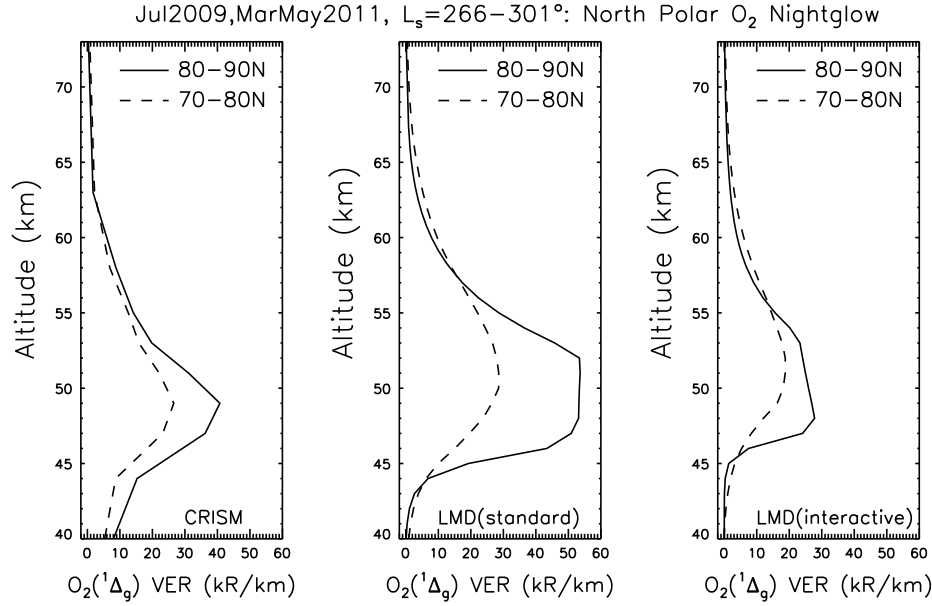


Figure 14. In the left panel, retrieved O₂(¹Δ_g) VER profiles are presented as averaged from 10 to 11 July 2009 ($L_s=301^\circ$); 31 March to 1 April 2011 ($L_s=265^\circ$); and 14–15 May 2011 ($L_s=293^\circ$) CRISM limb observations. CRISM limb observations at 70°N–80°N (dashed lines) and 80°N–90°N (solid lines) latitudes are compared to LMD GCM O₂(¹Δ_g) VER model profiles for standard (middle panel) and interactive aerosol (right panel) simulations averaged for the same L_s , LT, latitude, and longitude conditions for standard (middle panel) and interactive aerosol (right panel) simulations averaged for the same L_s , LT, latitude, and longitude conditions in this northern winter season.

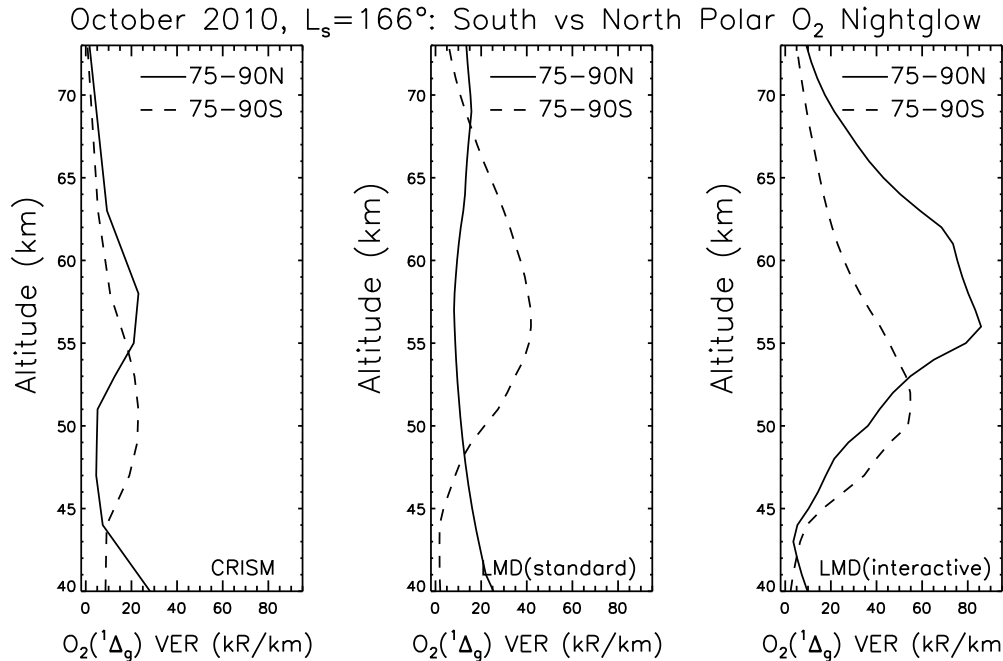


Figure 15. Averaged O₂(¹Δ_g) VER profiles are presented from 17 October 2010 ($L_s=166^\circ$) CRISM limb observations (left panel) at high southern (75°S–90°S, dashed lines) and high northern (75°N–90°N, solid lines), and compared to LMD O₂(¹Δ_g) VER model profiles for standard (middle panel) and interactive aerosol (right panel) simulations averaged for the same L_s , LT, latitude, and longitude conditions in this pre northern fall equinox, southern spring equinox period.

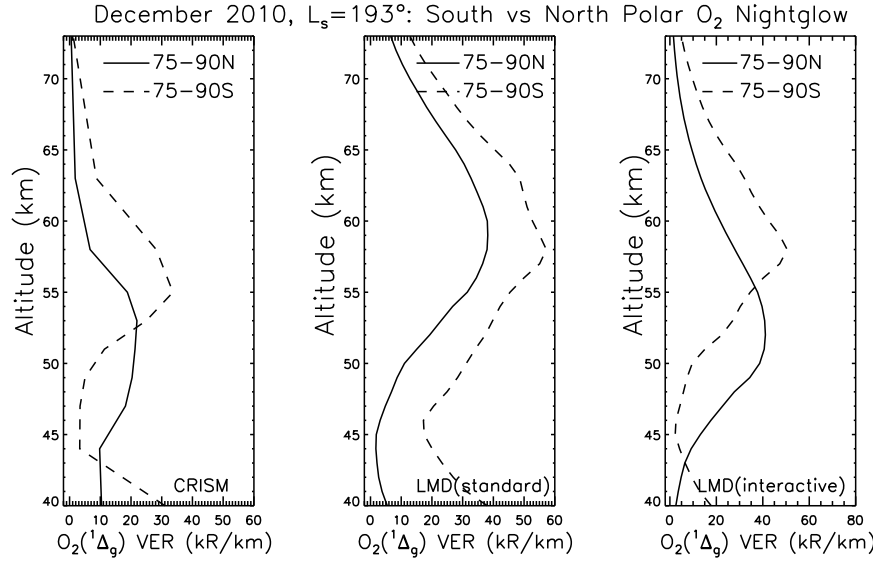


Figure 16. Averaged O₂(¹Δ_G) VER profiles are presented from 15 to 16 December 2010 ($L_s = 193^\circ$) CRISM limb observations (left panel) at high southern (75°S–90°S, dashed lines) and high northern (75°N–90°N, solid lines), and compared to LMD GCM O₂(¹Δ_G) VER model profiles for standard (middle panel) and interactive aerosol (right panel) simulations averaged for the same L_s , LT, latitude, and longitude conditions in this post northern fall equinox, southern spring equinox period.

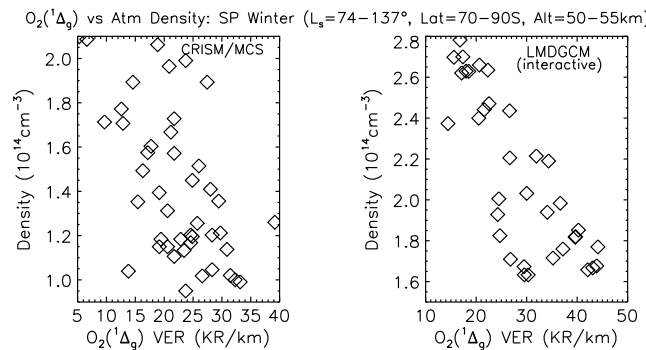


Figure 17. Observed atmospheric densities (from MCS) versus O₂(¹Δ_G) emission rates (from CRISM), averaged over the 50–55 km altitude region from April, May, and August ($L_s = 74\text{--}137^\circ$) periods of observation, are plotted in the left panel. The same interactive aerosol model quantities, selected as coincident with observed locations (latitude, longitude) and times (L_s , LT), are plotted in the right panel. Similar anticorrelations between atmospheric density and O₂(¹Δ_G) emission rates are presented by the observations and model. This counterintuitive behavior is associated with anti-correlation between atmospheric density and oxygen density (Figure 18, see text).

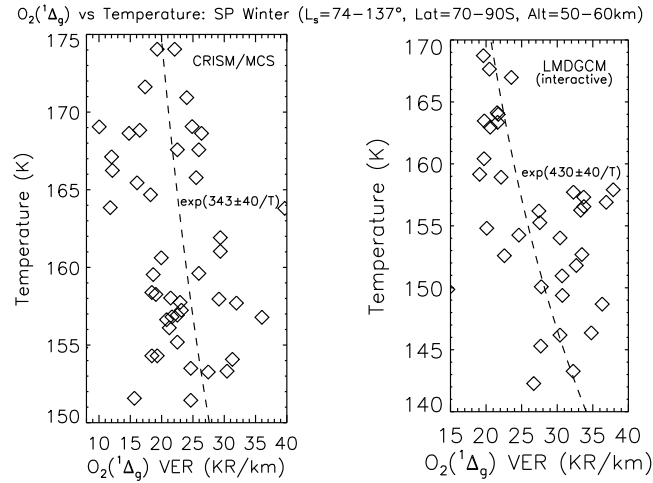


Figure 21. The correspondence between SP winter temperatures and O₂(¹Δ_g) 1.27 μm VER, as averaged over the 50–60 km altitude (aeroid) region for the CRISM locations (latitude = 70°S–90°S, all longitudes) and times (L_s , LT) of limb observations from April-to-August, 2010 (L_s = 74–137°). The left panel indicates an observed anticorrelation between colocated CRISM O₂(¹Δ_g) and MCS temperature observations. The right panel indicates similar anticorrelation between LMD GCM O₂(¹Δ_g) and temperature simulations. The dashed lines in both panels indicate a functional fit to the presented O₂(¹Δ_g) temperature distributions, assuming the $e^{(A/T)}$ dependence of the rate coefficient for winter polar O₂(¹Δ_g) formation (equation (1)). Similar fits are found for the observations and model, where the derived coefficients of 340–430 K compare to the adopted model temperature coefficient of 480 K or a more recent laboratory determination of 720 K by *Smith and Robertson [2008]* (see text).